

Active Visual SLAM with independently rotating camera

Elia Bonetto¹, Pascal Goldschmid^{2,1}, Michael J. Black¹ and Aamir Ahmad^{2,1}

Abstract—In active Visual-SLAM (V-SLAM), a robot relies on the information retrieved by its cameras to control its own movements for autonomous mapping of the environment. Cameras are usually statically linked to the robot’s body, limiting the extra degrees of freedom for visual information acquisition. In this work, we overcome the aforementioned problem by introducing and leveraging an independently rotating camera on the robot base. This enables us to continuously control the heading of the camera, obtaining the desired optimal orientation for active V-SLAM, without rotating the robot itself. However, this additional degree of freedom introduces additional estimation uncertainties, which need to be accounted for. We do this by extending our robot’s state estimate to include the camera state and jointly estimate the uncertainties. We develop our method based on a state-of-the-art active V-SLAM approach for omnidirectional robots, and evaluate it through rigorous simulation and real robot experiments. We obtain more accurate maps, with lower energy consumption, while maintaining the benefits of the active approach with respect to the baseline. We also demonstrate how our method easily generalizes to other non-omnidirectional robotic platforms, which was a limitation of the previous approach. Code and implementation details are provided as open-source.

I. INTRODUCTION

Using RGB cameras to allow a robot to simultaneously self-localize and map an environment is a popular approach [1]. There exist many passive V-SLAM methods that solve this problem, e.g. [2], [3], but active V-SLAM is gaining popularity [4], [5], [6] in recent years.

In general, the cameras are rigidly attached to the robot’s body constraining its *relative* orientation, even if some exceptions do exist since the seminal work of [7].¹ This design has several shortcomings. Firstly, it reduces the freedom of movement of the robotic platform. Having a fixed camera pose constrains the robot’s possible movement space not only for Active Visual-SLAM approaches like [4] but also next best view planners [5]. Indeed, having a robot that is capable of independently control the camera’s orientation increases its flexibility in both mapping and control.

Secondly, safety limits must be enforced to avoid collisions (with both environment and humans), and any possible tumble of the platform due to sudden changes in the velocities. This usually translate in low translation and



Fig. 1: Our omnidirectional robot actively mapping an office reception area.

rotation velocities that also reduce inertia-related movements. However, for the camera that is attached to an independent rotational joint, we can assume collision free movements and obtain a finer control due to the lighter system that needs to be rotated.

Thirdly, moving and rotating the robot imply a high energy consumption while rotating a system formed only by a camera is much more efficient.

Nonetheless, adding this additional degree of freedom introduce also a problem. The camera orientation w.r.t. the robot’s base should be expressed through an estimate and an uncertainty. Systems that utilize these kind of rotating cameras usually disregard this problem by assuming perfect calibration and high end encoders, or by ignoring the correlation between the two systems. These assumptions are usually costly, time consuming, and not always possible nor verifiable throughout the whole experiment. We address this issue by combining the camera and the robot’s pose estimates in an unified one that is then used by the system. This allows us not only to include all the information that we have with the corresponding uncertainty but also to not modify the underlying SLAM framework, thus keeping our method independent from it.

The summary of our contributions is as follows.

- We introduce a novel hardware architecture that allows us to address all the aforementioned restrictions, obtain more accurate maps and reduce energy consumption when used with [4].
- We expand the *iRotate* [4] method to different robotic platforms.
- We propose a novel odometry formulation for this kind of hardware architecture to obtain a more accurate map estimation.

We test the presented method both in simulation and on a real robot. We directly compare to [4] by using the same

¹Max Planck Institute for Intelligent Systems, Tübingen, Germany. firstname.lastname@tuebingen.mpg.de

²Institute for Flight Mechanics and Controls, The Faculty of Aerospace Engineering and Geodesy, University of Stuttgart, Stuttgart, Germany.

The authors thank the International Max Planck Research School for Intelligent Systems (IMPRS-IS) for supporting Elia Bonetto.

The authors would like to thank Heiko Ott and Mason Landry for their help with the design of the hardware.

¹Note that in hand-held mapping the camera is moving in a 3D world and represent the whole system

simulation environments, robot platform and parameters. The real robot, a Festo Didactic's Robotino, operates in an office environment (Fig. 1 and 2). The movement of the camera is controlled through a single low-cost incremental encoder. Our method's source code and instructions for use are available open-source².

The rest of the paper is structured as follows. In Sec. II we review the current state-of-the-art in independent camera movement. Our method is described thoroughly in Sec. III, while the experimental results are presented in Sec. IV. In Sec. V we conclude with comments on future work.

II. RELATED WORK

Optimized cameras' orientation has been used in many scenarios. From person tracking and surveillance [8], [9], [10], to next best view planning and active SLAM [4], [11], [12], [13], 3D reconstruction [14] and others.

Nonetheless, despite the clear advantages that controlling the camera's own direction brings, all those approaches usually lack either the independent camera orientation w.r.t. the robotic platform, or the simultaneous robot and camera's movements, or to address the uncertainty that the estimate of the camera's gaze might bring in the system.

In the simplest scenario the camera can be considered as the 'robotic' system itself, e.g. [9], [10], where the pan-tilt movement made by the camera is performed from a fixed global location. In those, even if it is the pan-tilt(-zoom) system of the camera that is being actively controlled, there is no other movement involved.

Other approaches, like [15], utilize the pan-tilt unit only during the calibration of the system while the robot is moving and localizing itself the (camera) orientation is kept fixed all the time. A notable exception is [14] where the authors propose a system of two RGB pan-tilt units that are used to gather only the color information that is then used for a 3D reconstruction system. In there, cameras can reach only a set pre-defined poses and with the use of high-accuracy encoders ensure high precision repeatability of those movements lacking any form of real activeness, SLAM capabilities, or simultaneous control of robot and camera's movement.

More advanced work, that include a simultaneous and independent movement of the camera with respect to the robot, are presented when humanoid robots are being employed as in [16]. There, the pan-tilt movement of the head, and therefore of the camera, is exploited to help robot's localization and tracking of targets. Moreover, the link between the two is not accounted for while the camera, and not the whole platform, is the focus of the working system that is employed in a partially-known environment.

In (active) visual SLAM most approaches rely to static cameras attached to the robotic system, thus, even if an active heading control is employed, it is the robot that rotates and not the camera. The seminal work from Davison [7] started the active feature tracking in SLAM, by using one

of the first independent rotating heading mechanism. This and the subsequent SLAM procedures developed by Davison et al. focus on the feature's tracking to reduce localization uncertainty applied to hand-held cameras. Fintrop et al. in [13] propose an actual active gaze control for SLAM using artificial landmarks, but do not introduce either a full active SLAM approach or a connection between camera's and robot's odometries. This work is very similar to [17], where Manderson et al. too actively control the gaze of the system while the navigation is performed by an external operator and the estimation is done for the camera frame itself. This implies that the system cannot be autonomous as it is proposed because the actual robot's orientation is unknown. Both these methods are more related to an active control of the camera rather than real active SLAM approaches. Even [18], where the camera system is controlled separately w.r.t. the robot, gaze prediction is agnostic about robot's movements and uses a greedy policy in the control, therefore lacking any link between the two and almost performing the two tasks separately. In [4] Bonetto et al. leverage the omnidirectional nature of the robot. In [5], instead, it is the high mobility of the drone that is being used to exploit a continuous change of heading limiting both approaches with respect to the considered platforms. Applying [4] to non-omnidirectional robot or [5] to other aerial vehicles like blimps is not straightforward without a separate camera control. Ultimately, to the best of our knowledge, there is yet no method that combines a full active SLAM approach with an active camera movement that is independent to the robotic platform *and* consider the system as a whole.

III. PROPOSED APPROACH

A. Problem Description and Notations

Let there be a robot, traversing on a 2D plane in a 3D environment, whose pose is given by $\mathbf{x}_R = [x_R \ y_R \ \theta_R]^\top$ and velocity by $\dot{\mathbf{x}}_R = [\dot{x}_R \ \dot{y}_R \ \dot{\theta}_R]^\top$. Let this robot be equipped with an RGB-D camera with an associated maximum sensing distance d_{thr} and horizontal field of view (FOV) α , a 2D laser range finder, and two IMUs units one of them attached to the camera and one on the robot's base. The camera is mounted on a joint that allows a full 360° independent rotation along the robot's z-axis, i.e. it has independent pan movement. We denote the orientation of the camera with respect to the robot as γ_C^R and its rotational velocity as $\dot{\gamma}_C^R$. Therefore, the orientation of the camera with respect to the world frame is $\psi = \theta_R + \gamma_C^R$ and its velocity is $\dot{\psi} = \dot{\theta}_R + \dot{\gamma}_C^R$.

Let then be $M \subset \mathbb{R}^2$ represent a bounded 2D grid map of the environment, where for each point $\mathbf{m} = [x_m \ y_m]^\top \in M$ we have an occupancy probability $p_o(\mathbf{m}) \in [0, 1]$. We assume that the robot begins exploration from a collision-free state and all map cells belong to the *unknown* space $M_{unk} \subset M$. The robot's goal is to autonomously map all the observable points in M_{unk} as *free* (M_{free}) or *occupied* (M_{occ}). At any given time instant the robot's state, map state and the set of observed visual features, and the graph \mathbf{G} of previously visited locations generated by the V-SLAM framework are available to the robot. A node $\mathbf{n} = [x \ y \ \theta]^\top \in \mathbf{G}$ is defined

²https://github.com/eliabntt/active_v_slam

by its coordinates in the map frame and by the orientation of the robot. While solving this problem, the robot must also be able to avoid both static and dynamic obstacles. The active SLAM approach used within the scope of this work is the one depicted in [4].

The goal is to use the camera's independent rotation to allow a simultaneous rotation of both the camera and the robot to reduce the overall energy consumption thanks to the increased freedom of movement. Moreover, we seek to apply [4] to different, non-omnidirectional, robotic platforms to increase the usability of that active V-SLAM method while keeping at least comparable performance. Moreover, we will study the effect that the merging of the estimation of the camera and the robot poses has, seeking better performance in terms of final map's entropy, accuracy and trajectory error w.r.t. the corresponding non-combined alternative.

B. Kinematic Description

The base of the robot used within this work is the same of [4], i.e. an omnidirectional three-wheeled robot. We can identify a distance D between the center of the robot and each wheel. The radius of the wheel r , and the angular position of the wheel $\alpha_i = i \cdot \frac{2}{3}\pi$ with $i \in [0, 1, 2]$. With $\mathbf{x}_G = [x_G \ y_G \ \theta_G]^\top$ and $\dot{\mathbf{x}}_G$, we indicate robot's position and velocity in the global frame. With these information we can obtain the kinematic model.

With \mathbf{T}_R we indicate the rotation matrix between the global and the local frame of the robot:

$$\mathbf{T}_R = \begin{bmatrix} \cos(\theta_G) & \sin(\theta_G) & 0 \\ -\sin(\theta_G) & \cos(\theta_G) & 0 \\ 0 & 0 & 1 \end{bmatrix}. \quad (1)$$

Moreover, \mathbf{S}_L denote the transformation from the robot's frame to each wheel:

$$\mathbf{S}_L = \begin{bmatrix} -\sin(\alpha_1) & \cos(\alpha_1) & D \\ -\sin(\alpha_2) & \cos(\alpha_2) & D \\ -\sin(\alpha_3) & \cos(\alpha_3) & D \end{bmatrix}. \quad (2)$$

We can obtain the wheel velocities $\omega = [\omega_1, \omega_2, \omega_3]$ with the following non linear relationship:

$$\omega = \mathbf{G} \cdot \mathbf{S}_L \cdot \mathbf{T}_R \cdot \dot{\mathbf{x}}_G, \quad (3)$$

where \mathbf{G} is the gear reduction ration matrix, i.e. a 3×3 diagonal matrix whose diagonal elements are all $1/r$.

With the introduction of the independent camera's control we introduce an additional degree of freedom. Then, by being $\dot{\gamma}_G$ the rotational velocity of the camera w.r.t. the robot in the global frame, we can control the system with $\dot{\mathbf{x}}'_G = [\dot{x}_G, \dot{y}_G, \dot{\theta}_G, \dot{\gamma}_G]^T$ and modify the just introduced matrices as follows.

$$\mathbf{T}'_R = \begin{bmatrix} & & 0 \\ & \mathbf{T}_R & \\ 0 & 0 & 1 \end{bmatrix}, \quad (4)$$

The last row links together the robot's and camera's rotations. Indeed, when the robot performs a rotation, that movement is transferred to the camera through the joint.

In both \mathbf{S}_L and \mathbf{G} the differences are minimal. Indeed,

$$\mathbf{S}'_L = \begin{bmatrix} & & 0 \\ & \mathbf{S}_L & \\ 0 & 0 & 1 \end{bmatrix}, \quad (5)$$

i.e. there is no transformation needed since the camera is centered with respect to the robot and \mathbf{G}' just introduce an element on the diagonal matrix.

Thus, we can define our system with

$$\omega' = \mathbf{G}' \cdot \mathbf{S}'_L \cdot \mathbf{T}'_R \cdot \dot{\mathbf{x}}'_G \quad (6)$$

C. Uncertainty

The considered SLAM framework, i.e. RTABMap [2], uses robot velocity's uncertainty in the links of the graph that is then used during the optimization phase.

Our system estimates the current state of both camera and robot. We assume that no ground truth data is available at any time. For both estimates we use a sensor fusion method based on EKF [19] to obtain position and velocity estimates along with their uncertainty. The robot's estimate is obtained using ICP odometry [20], the two IMUs and the wheel's odometry with an a-periodic refinement provided by the loop closures events used only for the x, y components for stability reasons. Thus, this state estimate is, in general, quite accurate over the whole experiment especially considering the velocity-related information.

For the camera's state estimation we are interested only on the *relative* yaw w.r.t. the robot's base. Note that we cannot directly use any of the two IMUs directly. Indeed, the IMU attached to the base of the robot will detect *only* the rotational movements of the robot while the one of the camera has no way to distinguish if it is the robot that rotates or if it is the camera itself. Therefore, we synchronize the two IMU sources and compute the instantaneous relative measurements. The error of this measurements is not the plain sum of uncertainties, which would be rather low, but is fixed at 0.01. This is because we recognize that, especially in the real world scenario, perfect synchronization is not possible and IMUs can drift and have high spikes in their readings. This generated 'differential' IMU is then fused in an EKF estimator with the encoder readings, successfully obtaining an estimate of the relative orientation of the camera with respect to the base of the robot.

The SLAM framework is designed to use *only* the robot's pose and uncertainty within the built graph while the camera relative pose is taken as a ground-truth. In other words, it is *not* possible to account for *both* the robot and the camera's uncertainties. The direct, and simpler, approach would be to neglect this and assume that the estimated camera orientation is indeed *always* correct. Nevertheless, we propose a novel solution to this problem. Instead of considering the two as separated entities, what we have done is to merge the two state estimates. In this, the position estimate is exactly the one obtained before while the orientation is obtained through the sum of both the camera and robot's yaw estimates. The same applies to velocities. Therefore, we are able to use,

within the RTABMap framework, a new ‘robot’ odometry that comprise both camera and robot estimations, i.e. the new odometry pose can be indicated by $\mathbf{x}_{sum} = [x_G, y_G, \psi]$ with the corresponding velocity $\dot{\mathbf{x}}_{sum}$ and the uncertainties computed as the sum of the single uncertainties.

In this way we achieve two goals: we successfully account for uncertainty introduced by the camera’s independent movement in the SLAM system and we do not need any modification of the considered framework. We can then use both approaches and compare the results.

D. Control and constraints

The work in [4] heavily rely on the assumption that the robot is omnidirectional. We can control such robot by using (3). To control the robot we utilize an NMPC formulation, generated by the ACADO framework [21]. We keep the system unchanged w.r.t. the one used in [4] with the same weights and penalties. The goal of the NMPC is to generate robot’s velocity commands in order to reach a predefined position and orientation. The robot has limits on velocities and can dynamically avoid obstacles. The NMPC thorough description is not depicted to avoid to introduce unnecessary confusion and further notation.

At first, we modify the NMPC formulation to account for 6. In this, the controlled orientation considered in the framework is the *final global* orientation of the *camera*. The penalty factor associated to the camera rotation is the same associated to the robot’s rotation. We use this formulation to test both a simultaneous rotation of the camera and the robot, and a scenario where only the camera is allowed to rotate. Note that with the latter we are effectively using a semi-holonomic robot that is capable to move only along x and y axis and, moreover, with this we linearize the whole system. Finally, to simulate a non-holonomic robot, we impose $v_y = 0$ for the whole duration of the experiment. For that to work we need to split control and enforce a smooth orientation of the robot base to follow the trajectory while the camera reach the desired orientation.

In all experiments we keep the same maximum rotational speed of the camera, of the robot, and also of the whole system.

IV. EXPERIMENTS AND RESULTS

Our robot, a Festo Didactic’s Robotino 1 (Fig. 2), has a 3-wheel omnidirectional drive base. We augmented the robot hardware with an extended physical structure containing a 2D laser range finder (Hokuyo A2M8) an IMU, an RGB-D camera (Intel RealSense D435i) with another embedded IMU unit, and a single-board computer (Intel(R) Core(TM) i7-3612QE CPU @ 2.10GHz). A virtual model of the same robot was created for the simulation experiments (Fig. 2 right).

A. Simulation Experiments

1) *Setup and Implementation*: For validation of the proposed algorithm we use the Gazebo simulator. We test our method in two different environments: i) AWS Robomaker

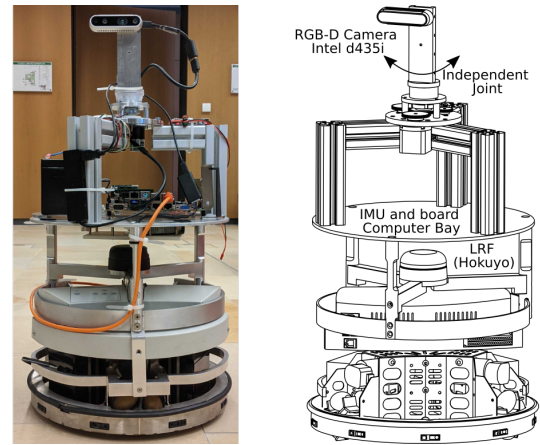


Fig. 2: Our robot platform – Festo Didactic’s Robotino with additional structure and hardware. Real robot (left), Gazebo model (right).

Small House World³ (Fig. 3a), which is $\sim 180m^2$, and ii) a modified version of the Gazebo’s Café environment (Fig. 3b) using 3DGems⁴ [22], which is $\sim 200m^2$.

We use real-hardware-like parameters for all the sensors in the simulation. The LRF has an angular resolution of 1° and provides a complete 360° sweep. The camera is used at the resolution of 848×480 . Its horizontal FOV is 69.4° , and maximum sensing depth is 4 meters. The NMPC horizon is 20 steps of 0.1s each. For all experiments the maximum translation speed of the robot is set to $1m/s$, while the maximum angular speed is $1rad/s$. The ground truth maps were obtained by using *pgm_map_creator*⁴ and edited to remove unwanted artifacts.

2) *Metrics*: We use RTAB-Map [2] as our V-SLAM back-end, which is a graph-feature-based visual SLAM framework. A 2D occupancy map is generated by the 2D projection of the 3D octomap built through our RGB-D sensor. This allows us to map the obstacles that would be otherwise hidden to the 2D LRF. Maps have a cell size of $0.05m$ and are compared w.r.t. the ground truth by using several metrics.

- The balanced accuracy score (BAC) on the three cells’ classes free, occupied and unknown
- root mean squared absolute trajectory error (ATE RMSE)
- the number of loop closures triggered per meter of distance traveled
- the wheels’ total overall rotation per meter traveled

With the last point we want capture the overall energy used by the robot throughout the experiment. Our hypothesis is that, by allowing the independent camera rotation, the system will be capable to balance the movement of both the robot and the independent joint more efficiently. A lower rotational movement of the wheels translate in less energy that has to be used to move the robotic platform. Map entropy is monitored throughout the entire experiment, and presented as normalized entropy w.r.t. the actual explored area.

³<https://github.com/aws-robotics/aws-robomaker-small-house-world>

⁴https://github.com/hyfan1116/pgm_map_creator



Fig. 3: Simulated Environments

3) *Comparisons*: The considered baseline for this work is *A_1_2_3* from [4]. All approaches are prefixed with A to indicate that we use all the three levels of activeness presented in [4]. We compare the baseline, named in this work *A_NC*, with our proposed merged state estimate (Subsec. III-C), which will be called A (without NC) in this work. The reason is that we are actually modifying the provided system uncertainty. With this test we can compare if there is any actual difference while we do *not* move the camera. In this way, we are able to create a baseline for the proposed moving camera approaches that utilize the same kind of information. Ideally, we should not observe any substantial difference.

Then, we compare our baseline against the different alternatives proposed in Subsec. III-D. We named these:

- HH: *both* the camera and the base can rotate at the same time with the *same* maximum speed
- OC: only the camera is allowed to rotate. The robot can only perform translational movements. This is a *semi-holonomic* scenario
- Y0: the robot is behaving as a *non-holonomic* robot, while the camera is allowed to rotate

In the first case we are introducing the additional degree of freedom, increasing the overall complexity of the system by adding an additional controlled variable. With the other two scenarios we are showing how the active SLAM approach is indeed usable even with other robotic platforms by removing the omnidirectional condition that was used.

Finally, we want also to study the effect that our proposed state estimate merging have in those method. As in the baseline case, the experiments that are suffixed with NC represent the standard approach while the ones without NC use our proposed state estimate.

Simulation results are averaged over 20 different successful trials of ten minutes each for each method with the same starting location on the map. Variability in trials is achieved as a result of different trajectories the robot takes in each one of the runs. Since RTABMap's execution rate is not fixed, but varies based on the movement of the robot, the plots are presented after post-processing of the data. This consists

of a bucketing procedure in time windows of 2 seconds, eventually filled with previous values. All comparisons are recapped in Tab. I.

	A	A_NC [4]	HH	HH_NC	OC	OC_NC	Y0	Y0_NC
Omnidirectional	✓	✓	✓	✓				
Camera rotating			✓	✓				
Semi-holonomic					✓	✓		
Non-holonomic							✓	✓
Merged estimate	✓		✓		✓		✓	

TABLE I: Considered comparisons

4) *Results*: Considering A and A_NC, it is clear from the experiments performed on both environments that our proposed way of merging state estimates do not alter the results w.r.t. the considered baseline. There are minimal differences in the mean and standard deviation values (see Tab. II and Tab. III), but nothing that indicates an overall change of performance. Thus, despite the fact that our merged odometry has a higher uncertainty in all the estimates, but especially in the yaw velocity, the SLAM framework remains unaffected. The final entropy, total path length, and exploration speed are similar among the two considered trials as depicted in Fig. 5 and Fig. 7. In this case, indeed, the camera was *not* performing independent rotational movements w.r.t. the base of the robot, and therefore, no difference was expected.

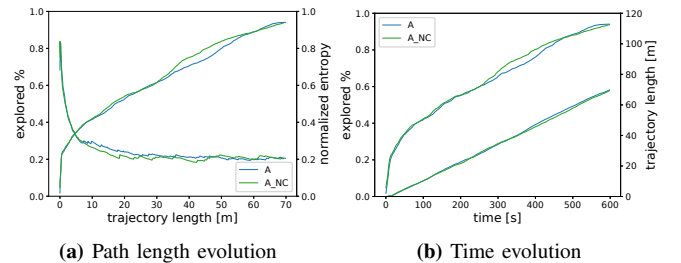


Fig. 4: Café: baseline and merged odometry

	BAC		Wheels' rotation per traveled meter		ATE RMSE		Loops per m	
	mean	std	mean [rad/m]	std [rad/m]	mean [m]	std [m]	mean	std
A	0.774	0.033	66.423	6.000	0.050	0.036	4.868	0.499
A_NC	0.771	0.022	65.781	5.000	0.059	0.028	4.965	0.596
HH	0.793	0.016	57.927	5.000	0.025	0.013	5.180	0.503
HH_NC	0.778	0.027	61.441	8.000	0.042	0.021	4.367	0.508
OC	0.784	0.024	55.494	5.000	0.027	0.034	7.608	0.699
OC_NC	0.755	0.040	56.064	6.000	0.038	0.035	7.081	0.607
Y0	0.728	0.033	55.770	3.000	0.022	0.006	7.452	0.577
Y0_NC	0.705	0.058	57.774	7.000	0.031	0.018	9.486	1.119

TABLE II: Café environment experiment results

When the rotation of the camera is introduced there are some interesting results. First of all, if we compare the two state estimate definitions we can see how, among all experiments, the classical way of considering the camera rotation as perfectly known is worse. This can be seen in both the environments considered, looking either at the tables Tab. III and Tab. II or at the figures Fig. 7 or Fig. 5. Among all experiments we observe an improvement of the overall balanced accuracy between 1.5% and 5% comparing the merged state estimate experiments against the NC counterparts. ATE is also reduced (between 10% and 40% lower) while also loop closures are more frequent (between 10% and 30% higher) except in the non-holonomic case. However, the higher number of loop closures of Y0_NC w.r.t.

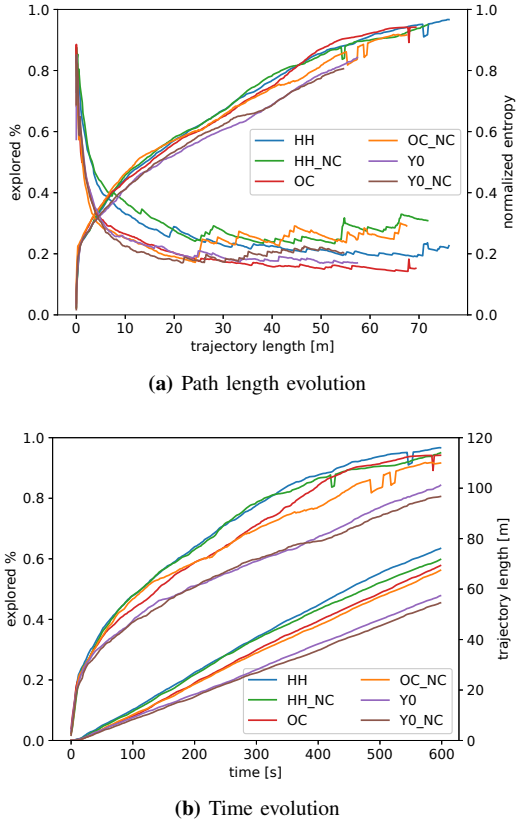


Fig. 5: Caf : different robotic platforms

Y0 do not positively affect the system and it is most probably linked to the lower area explored with the same amount of movement of the platform. The greatest difference can be seen once we compare the entropy evolution. In this, when we compare the merged state estimate approach w.r.t. the NC counterparts for all the platforms (HH, OC and Y0) we can see how the initial evolution is comparable in the first 20m of the trajectory and, after this point, the approaches diverge. The bigger difference can be observed in both the couples HH-HH_NC and OC-OC_NC. Finally, Y0 shows the smallest difference in terms of normalized entropy but it has also the shortest traveled path. The trend is clearly divergent with our approach performing better w.r.t. Y0_NC. Clearly, it is true that the active SLAM method has influence w.r.t. entropy evolution but, since the exploration profile are equivalent between all the alternative w.r.t. their NC counterparts, we can safely infer that the difference in the performance is not due to this building block. Most likely, the main problem here is that the robot register an orientation for the camera and, when loop closures happen, the drift and the uncertainty that are not taken into account have a clear effect on the overall final estimation procedure.

Comparing the three robotic platforms w.r.t. the baseline we notice how, overall, our active SLAM approach presented in [4] is indeed usable with different robotic platforms. The first thing that is clear is the overall energy reduction that our approach proposed in this work brings. When we rotate both robot and camera, even if we maintain the coupled maximum rotational speed, the system achieves 20% less

total wheel rotation per meter traveled. This implies that the rotation of the camera is capable of reducing the rotation of the robot, further optimizing its movements. This is indeed reflected in every considered metric and in the fact that we perform 10% longer paths within the same time window, suggesting a better optimization and faster reaching of the desired waypoints' orientations. Anyway, this does not reflect in longer paths since the exploration profiles are comparable.

Moreover, we can see how the semi-holonomic robot (OC) is capable of obtaining even better performance obtaining a lower normalized entropy while keeping a low wheels' rotation amount. In terms of ATE and BAC it is quite similar to the HH method, underperforming slightly in the Caf  environment while getting better results in the Small House. In this case, avoiding the rotation of the base of the robot brings a higher number of loop closures, probably linked to the fact that it is easier for the system to match 2D laser scans. Altogether, these factors indeed help the system in achieving these results. One should also note that, in this scenario, the RTABMap system actually 'thinks' that the robot is rotating during the experiment, further proving the goodness of both camera rotation (in terms of efficiency) and of our merged odometry system. It is worth noticing that without the camera rotation, a holonomic robot would have a very inefficient start and stop behaviour to follow the desired heading that continuously changes along the trajectory.

Finally, the non-holonomic robot (Y0 and Y0_NC), is the worse in terms of BAC. This is probably linked to the fact that it is capable of exploring a much lower amount of area that, clearly, lower the balanced accuracy performance. In this case, we should also take into account that we did not optimize trajectory or waypoints for a non-holonomic robot because we wanted to keep the comparison as fair as possible. We believe that performing such optimization would be indeed beneficial, especially in the total amount of explored area. The higher number of loop closures of Y0_NC can be linked to the slow movement and the lower amount of area seen despite the comparable path length. Anyway, taking into account also the other metrics it seems reasonable to say that Y0 performs better overall.

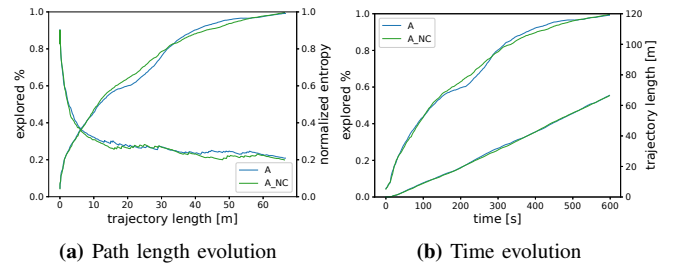
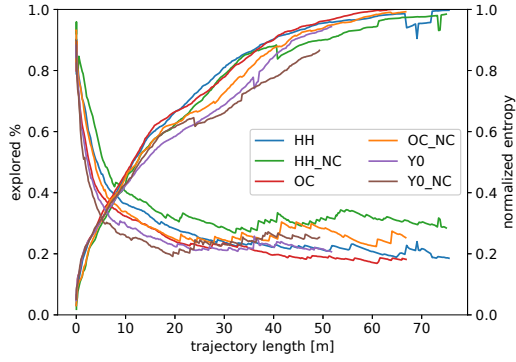


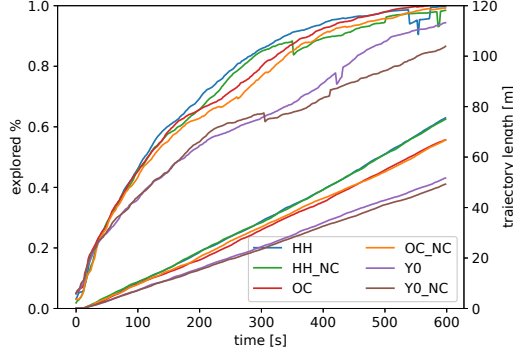
Fig. 6: Small house: baseline and merged odometry

B. Real Robot Experiments

The real robot environment has been reconstructed similarly to the one used in [4]. The experiments consist in five runs of five minutes each. Difference between the results of our baseline (A_NC) and the results of the same approach



(a) Path length evolution



(b) Time evolution

Fig. 7: Small house: different robotic platforms

	BAC		Wheels' rotation per traveled meter		ATE RMSE		Loops per m	
	mean	std	mean [rad/m]	std [rad/m]	mean [m]	std [m]	mean	std
A	0.810	0.019	64.514	5.000	0.056	0.031	4.634	0.525
A_NC	0.818	0.015	63.043	3.000	0.051	0.020	4.692	0.382
HH	0.825	0.017	53.635	3.000	0.027	0.013	4.788	0.398
HH_NC	0.808	0.014	54.618	5.000	0.038	0.016	3.659	0.492
OC	0.832	0.012	50.232	2.000	0.026	0.017	7.447	0.742
OC_NC	0.811	0.018	51.257	3.000	0.030	0.014	6.597	0.716
Y0	0.785	0.029	56.059	2.000	0.032	0.009	7.334	0.532
Y0_NC	0.742	0.047	61.938	12.000	0.035	0.022	9.642	1.422

TABLE III: Small house environment experiment results

presented in [4] are to be linked to the different environment set-up that caused different paths and to the estimation of the rotation of the camera w.r.t. the base of the robot. Those two main factors combined caused a lower number of loop closures and an higher map entropy. Moreover, since wheels' encoder readings are not available, we can not directly compare the wheel rotational movement per meter travelled. Nonetheless, to give an approximation of how the robot behave between the graph nodes constructed by the RTABMap we computed the total rotation of the base of the robot and of the camera. Note that this measurement is not fully indicative of how much the robot rotates *between* nodes. Furthermore, the encoder necessary to read and refine the camera rotational movement through the EKF was not available leaving the estimated relative rotation to the two IMUs. The PID used caused a considerable delay any time it had to initiate the rotation of the camera. Finally, while the linear speed is the same of the previously run experiments, i.e. 0.3 m/s , the angular speed has been increased to 1 rad/s (from 0.5) which caused the robotic platform to perform more harsh and inaccurate rotational movements.

From the exploration profile and the normalized entropy

graphs we can notice that the algorithm presented in [4] is applicable to a semi-holonomic platform (OC, OC_NC) without losing generality. The ease of control, the fact that the RTABMap is not aware of the noise related to the camera orientation are to be linked to the outperforming exploration speed of OC_NC.

Comparing the total estimated rotation, even when the system is forced to not rotate one of the two components (i.e. A_NC, OC_NC), it estimate 0.23 radians per meter travelled of rotation while ideally this number should be 0 . Thus, it is clear how the system has in this scenario more difficulties to estimate the map (higher entropy) and recognize places (lower loop closures) w.r.t. the work in [4] (which had a static camera). HH_NC base's rotation amount is comparable to A_NC due to the aforementioned PID's delay that has to be compensated by the robot's rotational movement. Despite that, HH_NC shows some benefits even in these short term experiments by having shorter paths w.r.t. A_NC but with higher exploration speed. Thus, rotating both the camera and the robot, apart from having a theoretical energy saving advantage and despite the higher control complexity can bring also a benefit on the overall system. OC_NC is less affected by the PID delay because the continuous rotation input from the MPC cause the camera to almost never stop. In that case, the PID behaves quite well since there is no need to build up the initial movement. We can also notice how the rotational movement per meter is higher in both OC_NC and HH_NC showing a more effective control strategy.

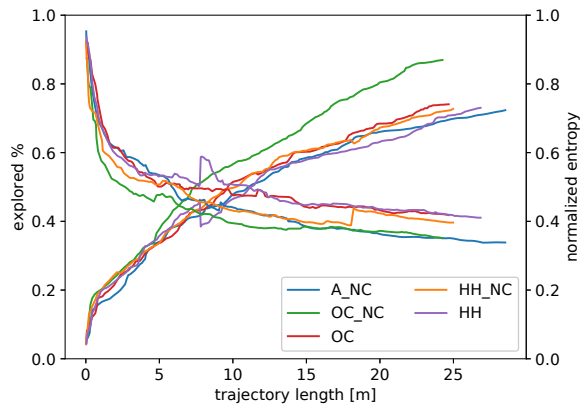
Finally, it is interesting to notice that, despite not being perfectly estimated, the method of merging the state estimates seems promising. We can see from Tab. IV that the loop closures benefit from this kind of representation even if the added noise degrades the estimation of the map in terms of normalized entropy by a small amount (5% , see Fig. 8). The bigger difference can be seen comparing OC and OC_NC but, as mentioned before, the performance of OC_NC could be a bit misleading on its own. Overall, given some limitations of our hardware platform, these results show both the usefulness of our approach to different robotic platforms, the benefits of rotating both the camera and the robot simultaneously and the goodness of the proposed merging strategy for state estimates.

		A_NC	OC_NC	OC	HH_NC	HH
Area	mean [m^2]	72.348	86.973	74.072	72.729	73.033
	std [m^2]	8.710	7.397	12.473	7.903	12.496
Robot's rotation	mean [rad/m]	1.675	0.228	3.070	1.684	2.804
	std [rad/m]	0.250	0.032	0.313	0.362	0.960
Camera's rotation	mean [rad/m]	0.227	2.580	—	1.419	—
	std [rad/m]	0.023	0.456	—	0.839	—
Path Length	mean [m]	28.526	24.255	24.677	24.978	26.846
	std [m]	2.516	3.093	2.231	6.794	4.128
Loops per m	mean	0.370	0.920	2.200	0.820	1.570
	std	0.470	0.900	1.530	0.650	2.300

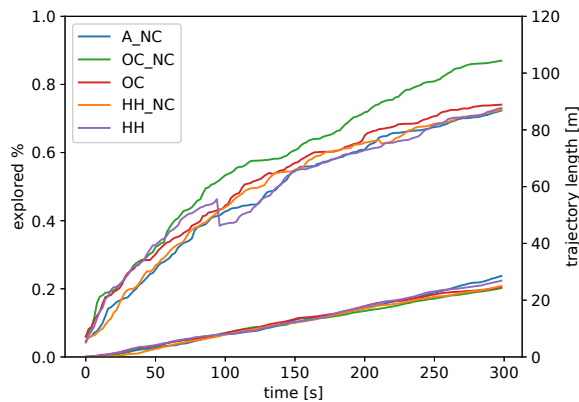
TABLE IV: Real robot experiments

V. CONCLUSIONS

In this work we have shown how we can apply *iRotate* to different robotic platforms, allowing us to use this active SLAM algorithm with a variety of robots and dismissing the omnidirectional requirements. While mapping performance



(a) Path length evolution



(b) Time evolution

Fig. 8: Real robot experiments

are not being affected by the robotic platform itself it has been shown how an independent camera rotation yield lower energy consumption either because it facilitate the robot's own rotation or because we can utilize a non-holonomic platform.

Moreover, the proposed merged odometry has shown promising results in both simulation and real world experiments despite the limitation of the latter ones.

Note that, using a 'full' holonomic robot could further optimize the energy consumption in that scenario. A small in-place rotation could indeed align the robot with the movement direction, thus avoiding the rotation movement of one of the wheels. Also with respect to HH a diversified control strategy in which energy efficiency is sought for the base and the camera is responsible to reach the desired orientation could further reduce the overall energy consumption of the system.

REFERENCES

- [1] C. Cadena, L. Carlone, H. Carrillo, Y. Latif, D. Scaramuzza, J. Neira, I. Reid, and J. J. Leonard, "Past, present, and future of simultaneous localization and mapping: Toward the robust-perception age," *IEEE Transactions on Robotics*, vol. 32, no. 6, pp. 1309–1332, 2016.
- [2] M. Labbé and F. Michaud, "Rtab-map as an open-source lidar and visual simultaneous localization and mapping library for large-scale and long-term online operation," *Journal of Field Robotics*, vol. 36, no. 2, pp. 416–446, 2019. [Online]. Available: <https://onlinelibrary.wiley.com/doi/abs/10.1002/rob.21831>

- [3] A. Rosinol, M. Abate, Y. Chang, and L. Carlone, "Kimera: an open-source library for real-time metric-semantic localization and mapping," in *2020 IEEE International Conference on Robotics and Automation (ICRA)*, 2020, pp. 1689–1696.
- [4] E. Bonetto, P. Goldschmid, M. Pabst, M. J. Black, and A. Ahmad, "iRotate: Active Visual SLAM for Omnidirectional Robots," 2021.
- [5] C. Papachristos, S. Khattak, and K. Alexis, "Uncertainty-aware receding horizon exploration and mapping using aerial robots," in *2017 IEEE International Conference on Robotics and Automation (ICRA)*, 2017, pp. 4568–4575.
- [6] A. Kim and R. M. Eustice, "Active visual slam for robotic area coverage: Theory and experiment," *The International Journal of Robotics Research*, vol. 34, no. 4-5, pp. 457–475, 2015. [Online]. Available: <https://doi.org/10.1177/0278364914547893>
- [7] A. J. Davison and D. W. Murray, "Mobile robot localisation using active vision," in *Computer Vision — ECCV'98*, H. Burkhardt and B. Neumann, Eds. Berlin, Heidelberg: Springer Berlin Heidelberg, 1998, pp. 809–825.
- [8] Hyukseong Kwon, Youngrock Yoon, Jae Byung Park, and A. C. Kak, "Person tracking with a mobile robot using two uncalibrated independently moving cameras," in *Proceedings of the 2005 IEEE International Conference on Robotics and Automation*, 2005, pp. 2877–2883.
- [9] A. Del Bimbo, G. Lisanti, I. Masi, and F. Pernici, "Continuous recovery for real time pan tilt zoom localization and mapping," in *2011 8th IEEE International Conference on Advanced Video and Signal Based Surveillance (AVSS)*, 2011, pp. 160–165.
- [10] P. Carr, M. Mistry, and I. Matthews, "Hybrid robotic/virtual pan-tilt-zoom cameras for autonomous event recording," in *Proceedings of the 21st ACM international conference on Multimedia*, 2013, pp. 193–202.
- [11] A. Dai, S. Papatheodorou, N. Funk, D. Tzoumanikas, and S. Leutenegger, "Fast frontier-based information-driven autonomous exploration with an mav," in *2020 IEEE International Conference on Robotics and Automation (ICRA)*, 2020, pp. 9570–9576.
- [12] L. Schmid, M. Pantic, R. Khanna, L. Ott, R. Siegwart, and J. Nieto, "An efficient sampling-based method for online informative path planning in unknown environments," *IEEE Robotics and Automation Letters*, vol. 5, no. 2, pp. 1500–1507, 2020.
- [13] S. Frintrop and P. Jensfelt, "Attentional landmarks and active gaze control for visual slam," *IEEE Transactions on Robotics*, vol. 24, no. 5, pp. 1054–1065, 2008.
- [14] K. Pervolz, A. Nuchter, H. Surmann, J. Hertzberg, and S. Birlinghoven, "Automatic reconstruction of colored 3d models," *VDI BERICHTE*, vol. 1841, pp. 215–222, 2004.
- [15] A. Zdešar, G. Klančar, and I. Škrjanc, "Vision-based localization of a wheeled mobile robot with a stereo camera on a pan-tilt unit," in *ICINCO*, 2019.
- [16] M. Mattamala, C. Villegas, J. M. Yáñez, P. Cano, and J. Ruiz-del Solar, "A dynamic and efficient active vision system for humanoid soccer robots," in *RoboCup 2015: Robot World Cup XIX*, L. Almeida, J. Ji, G. Steinbauer, and S. Luke, Eds. Cham: Springer International Publishing, 2015, pp. 316–327.
- [17] T. Manderson, F. Shkurti, and G. Dudek, "Texture-aware slam using stereo imagery and inertial information," in *2016 13th Conference on Computer and Robot Vision (CRV)*. IEEE, 2016, pp. 456–463.
- [18] G. Lidoris, K. Kuhnlenz, D. Wollherr, and M. Buss, "Combined trajectory planning and gaze direction control for robotic exploration," in *Proceedings 2007 IEEE International Conference on Robotics and Automation*, 2007, pp. 4044–4049.
- [19] T. Moore and D. Stouch, "A generalized extended kalman filter implementation for the robot operating system," in *Proceedings of the 13th International Conference on Intelligent Autonomous Systems (IAS-13)*. Springer, July 2014.
- [20] F. Pomerleau, F. Colas, R. Siegwart, and S. Magnenat, "Comparing ICP Variants on Real-World Data Sets," *Autonomous Robots*, vol. 34, no. 3, pp. 133–148, Feb. 2013.
- [21] B. Houska, H. J. Ferreau, and M. Diehl, "Acado toolkit—an open-source framework for automatic control and dynamic optimization," *Optimal Control Applications and Methods*, vol. 32, no. 3, pp. 298–312, 2011. [Online]. Available: <https://onlinelibrary.wiley.com/doi/abs/10.1002/oca.939>
- [22] A. Rasouli and J. K. Tsotsos, "The effect of color space selection on detectability and discriminability of colored objects," *arXiv preprint arXiv:1702.05421*, 2017.